

Carbon Nanotube/Biocompatible Bola-Amphiphile Supramolecular Biohybrid Materials: Preparation and Their Application in Bacterial Cell Agglutination

Guocan Yu, Jinying Li, Wei Yu, Chengyou Han, Zhengwei Mao, Changyou Gao, and Feihe Huang*

The excellent electronic conductivity, chemical inertness, mechanical toughness, and elasticity of carbon nanotubes (CNTs) have enabled a wide range of opportunities and potential applications in biology and medicine, for example in biosensors, electroanalytical nanotube devices, artificial muscles, and laser heating cancer therapy.^[1] However, the construction of biomaterials based on CNTs is greatly limited as a result of their lack of solubility in water. Recently, various methods have been developed to solubilize CNTs in water.^[2,3] Covalent functionalization improves the water-solubility of CNTs, but it often leads to disruption of the extended π -networks on their surfaces, resulting in diminishing both their mechanical and electronic properties.^[2] On the other hand, supramolecular approaches to solubilize CNTs in water can preserve the unique properties of CNTs. Therefore, they have attracted much interest in the last decade.^[3] Polymers, surfactants, peptides, nucleic acids, and proteins have all been used to wrap CNTs through non-covalent functionalization in order to improve their water solubility.

However, the improvement of the water solubility is not enough for the successful fabrication of biomaterials based on CNTs. The achievement of biocompatible interactions between CNTs and living cells is also required. For this purpose, positively charged polyelectrolytes, such as poly(ethyleneimine) and poly-L-lysine, have been used to coat hydrophobic CNTs to promote adhesion to the negatively charged cell membrane. However, the resultant non-physiological, strong electrostatic interactions may lead to cell death or cytotoxic effects.^[3b,4] Therefore, in order to ensure biocompatible interactions between CNTs and living systems and preserve the functionalities of both in the fabrication of CNT-based biomaterials, new strategies are needed.

Herein we report a new strategy to prepare CNT-based biomaterials by hybridizing biocompatible bola-amphiphiles

with CNTs. Three different bola-amphiphiles, NP1, NP2, and ND, were designed and synthesized. They contain electron-rich naphthalene (NP1 and NP2, which refer to the 1,5- and 2,6-substitutions of naphthalene, respectively) or electron-deficient naphthalene diimide (ND) groups in their hydrophobic parts and biocompatible galactoses in their hydrophilic parts (Figure 1). The π - π interactions between the aromatic naphthalene or naphthalene diimide groups in the hydrophobic parts of the bola-amphiphiles and CNTs can be used to achieve hybridization, while the hydrophilic parts containing galactose groups can be utilized to solubilize the CNTs in water and to endow these biohybrid materials with biocompatible interactions with living cells. Three supramolecular biohybrid materials based on single walled carbon nanotubes (SWNTs) and these biocompatible bola-amphiphiles were prepared and their application in bacterial cell agglutination was investigated.

First, we wanted to understand how these three bola-amphiphiles self-assemble in water. From Figure 2a and b, the critical aggregation concentrations (CAC) of NP1 and NP2 were determined to be 5.12×10^{-4} and 3.22×10^{-4} M, respectively, using concentration-dependent conductivity. Transmission electron microscopy (TEM) experiments assisted in the visualization of the self-assembled nanostructures of NP1 and NP2. As shown in Figure 2d, solid spherical structures were formed by NP1 with an average diameter of about 180 nm when the concentration was higher than its CAC value. Dynamic light scattering (DLS) was employed to confirm the size of the spherical structures. As shown in Figure 2g, the mean diameter of the aggregates formed by NP1 alone was 190 nm, in good agreement with the corresponding TEM image shown in Figure 2d. It should be pointed out that the diameter of the nano-aggregates measured by DLS was little larger than that observed in the TEM images. This was attributed to the swelling effect of the spherical structures in water.^[5] Likewise, solid spherical structures were formed by NP2 alone with a similar average diameter observed by TEM (Figure 2e) and verified by DLS (Figure 2h).

On the other hand, the CAC value of ND was determined to be 2.96×10^{-4} M (Figure 2c), which is lower than those of NP1 and NP2 due to much stronger π - π stacking interactions between naphthalene diimide units in water.^[6] Compared with the self-assemblies formed by NP1 and NP2, the distinct morphology of the self-assemblies formed by ND could be seen in the TEM image. ND self-assembled into one-dimensional nanostructures of about 6–8 nm in diameter and several hundred nanometers in length (Figure 2f). There was no sharp color

Prof. G. Yu, J. Li, F. Huang, C. Han
MOE Key Laboratory of Macromolecular Synthesis
and Functionalization
Department of Chemistry
Zhejiang University
Hangzhou, 310027, P. R. China
E-mail: fhuang@zju.edu.cn

W. Yu, Prof. Z. Mao, C. Gao
MOE Key Laboratory of Macromolecular Synthesis
and Functionalization
Department of Polymer Science and Engineering
Zhejiang University
Hangzhou, 310027, P. R. China



DOI: 10.1002/adma.201302942

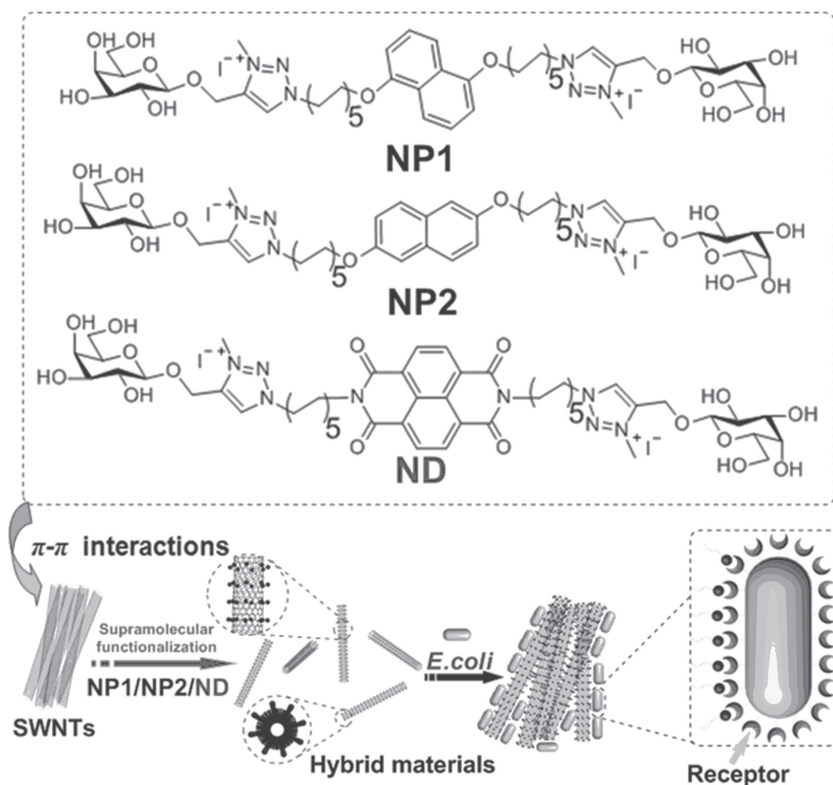


Figure 1. Molecular structures of the bolaform amphiphiles **NP1**, **NP2**, and **ND** and a schematic representation of the biohybrid material preparation through a supramolecular approach and their application in *Escherichia coli* agglutination.

contrast between the periphery and central parts, suggesting that the one-dimensional nanostructures were solid nanorods (rod-like micelles).^[6b]

In addition, ¹H NMR studies provided convincing information about the self-assembly behaviors of **NP1**, **NP2**, and **ND** in water. Compared with the resonances related to the protons of the bolaform amphiphiles alone conducted in DMSO-*d*₆ (Figure S37, Supporting Information), broadening of all signals in D₂O at the same concentration was clearly observed for the amphiphiles themselves, indicating the formation of large aggregates,^[7e] which was driven by π - π interactions between the aromatic rings and hydrophobic interactions between the alkyl chains.^[7]

Three biohybrid materials, **NP1**/SWNTs, **NP2**/SWNTs, and **ND**/SWNTs, were then prepared by simple sonication of **NP1** (**NP2** or **ND**) (20.0 mg) in H₂O (5.00 mL) with 1.00 mg of SWNTs. During the sonication, the aqueous solution changed from colorless to black, indicating solubilization of the SWNTs. Insoluble SWNTs were removed by centrifugation and the supernatant containing the bola-amphiphiles was dialyzed against H₂O for two weeks to remove excess free **NP1** (**NP2** or **ND**) from the solution. The black solution of the respective hybrid material was homogeneous and stable, and could stand over 1 month without significant changes. This observation indicated that **NP1** (**NP2** or **ND**) played an important role in the solubilization of SWNTs. Direct evidence for successful

preparation of hybrid materials stemmed from TEM observations which assisted in the visualization of the SWNTs. TEM images of pristine SWNTs showed the presence of large aggregates of nanotubes (Figure 3a), while for the hybrid materials, individual SWNTs of 2–3 nm in diameter could be clearly observed (Figure 3b, c, d). As shown in the TEM images, the bolaform amphiphiles (marked by blue or red arrows) wrapped the SWNTs tightly. The presence of well dispersed SWNTs proved that our non-covalent approach could solubilize SWNTs through π - π interactions effectively in aqueous solution, resulting in the dispersion of SWNTs from their original bundles.

To confirm the formation of π - π interactions between SWNTs and the bolaform amphiphiles (**NP1**, **NP2**, or **ND**), fluorescence spectroscopy was employed to monitor the difference in fluorescence emission between the solution of bola-amphiphiles alone and the aqueous dispersion of SWNTs. As shown in Figure S39, Supporting Information, a solution of **NP1** displayed the characteristic fluorescence emission of naphthalene groups with high intensity. However, strong fluorescence quenching was observed upon gradual addition of SWNTs.^[3e] The quenching was attributed to the interactions between **NP1** and SWNTs and energy transfer from the naphthalene to SWNTs through π - π interactions. Similar phenomena were observed when **NP1** was replaced by **NP2** (Figure S40, Supporting Information) or **ND** (Figure S41, Supporting Information), confirming the effective π - π interactions between the bola-amphiphiles and SWNTs. Moreover, exact evidence for the successful preparation of hybrid materials was obtained by utilizing UV-vis-NIR spectroscopy. Figure 3e shows the UV-vis-NIR spectrum of the **NP1**/SWNTs hybrid. In the range of 900–1300 nm, typical SWNTs van Hove singularities were found, which were not observable for SWNTs alone caused by their poor solubility.^[2b] The characteristic absorptions were observed in the UV-vis-NIR spectra (Figure S42 and S43, Supporting Information) of the **NP2**/SWNTs and **ND**/SWNTs hybrids, indicating the homogeneous dispersion of SWNTs.^[2b]

Furthermore, thermal gravimetric analysis (TGA) was employed to confirm whether the bola-amphiphile modified the SWNTs and to calculate the respective content of the organic compounds in the hybrid systems. The original untreated SWNTs were also studied as a control experiment. Compared with the original SWNTs (Figure S44, Supporting Information), **NP1**/SWNTs underwent 50.2% weight loss up to 630 °C corresponding to the decomposition temperature of SWNTs (Figure 3f). This TGA result provided additional evidence of the existence of **NP1** in the hybrid material. The contents of **NP2** and **ND** in their hybrids were calculated to be 54.2% (Figure S45, Supporting Information) and 65.4% (Figure S46,

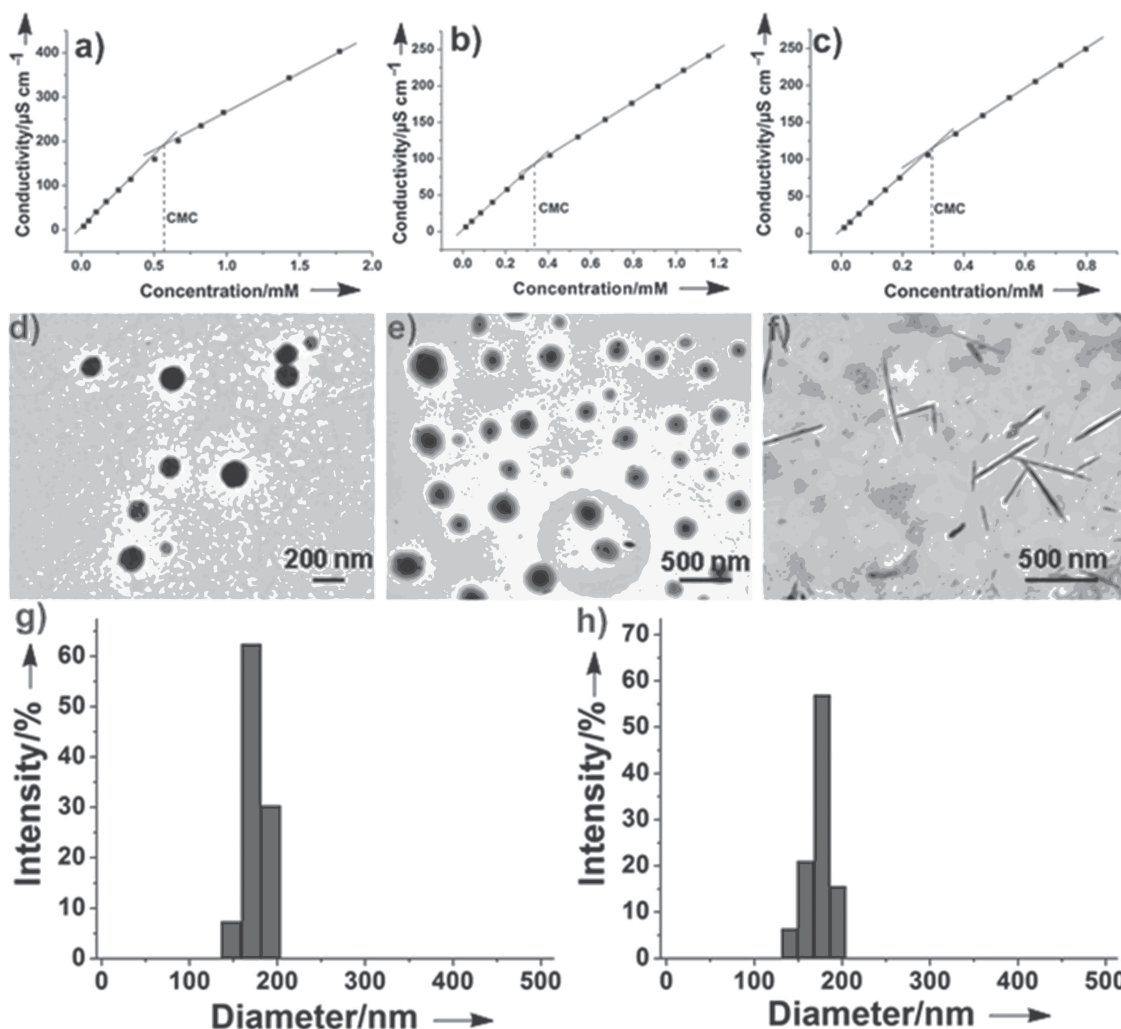


Figure 2. The concentration-dependent conductivities of a) NP1, b) NP2, and c) ND. TEM images of d) NP1, e) NP2, and f) ND. DLS results of g) NP1 and h) NP2. The CACs were determined to be 5.12×10^{-4} , 3.22×10^{-4} , and 2.96×10^{-4} M for NP1, NP2, and ND, respectively. The solution concentrations for the TEM experiments were 1.00×10^{-3} M for NP1, NP2, and ND, which were higher than the CAC values of the corresponding bolaform amphiphiles.

Supporting Information), respectively. These results indicated that the bola-amphiphiles (NP1, NP2, and ND) containing aromatic rings had strong abilities to keep the SWNTs well-dispersed in water through non-covalent interactions, forming novel supramolecular biohybrid materials.

Recently, materials scientists and chemists have shown considerable interests in understanding and mimicking bacterial adhesin-specific interactions for various purposes, such as pathogen detection and the inhibition of bacterial infections by the chemotactic responses of bacteria toward the corresponding ligands (such as carbohydrates).^[8] Typically, carbohydrate-protein interactions exhibit high specificity and weak affinities toward corresponding ligands or receptors, always in the millimolar range.^[9] To circumvent this problem and to function as potent and specific effectors or inhibitors of biological processes, multivalent or cluster effects, which are much stronger than the corresponding monovalent interactions,

have been employed to enhance the binding efficiency.^[10] It has been reported that multivalent carbohydrate-coated self-assemblies can induce agglutination and inhibit the motility of pathogenic cells, such as *Escherichia coli*.^[11] In the biohybrid materials prepared here, the existence of rich galactose surfaces on the aggregates should provide a multivalent ligand that has a high affinity for carbohydrate receptors. On the other hand, in vitro cytotoxicity studies displayed low toxicities of NP1, NP2, and ND to A549 cells (Figure S38, Supporting Information), which provided convincing indemnification for the application of these bolaform amphiphiles in biologically relevant fields. Therefore, optical microscopy, fluorescence microscopy, and TEM were employed to investigate the ability of the hybrid materials to agglutinate *E. coli* cells. Unexpectedly, when *E. coli* was cultured with any of the bolaform amphiphiles alone, absolutely no clusters of fluorescent bacteria of different sizes were observed (Figure 4a, d, g and Figure 4b, e, h). TEM was also

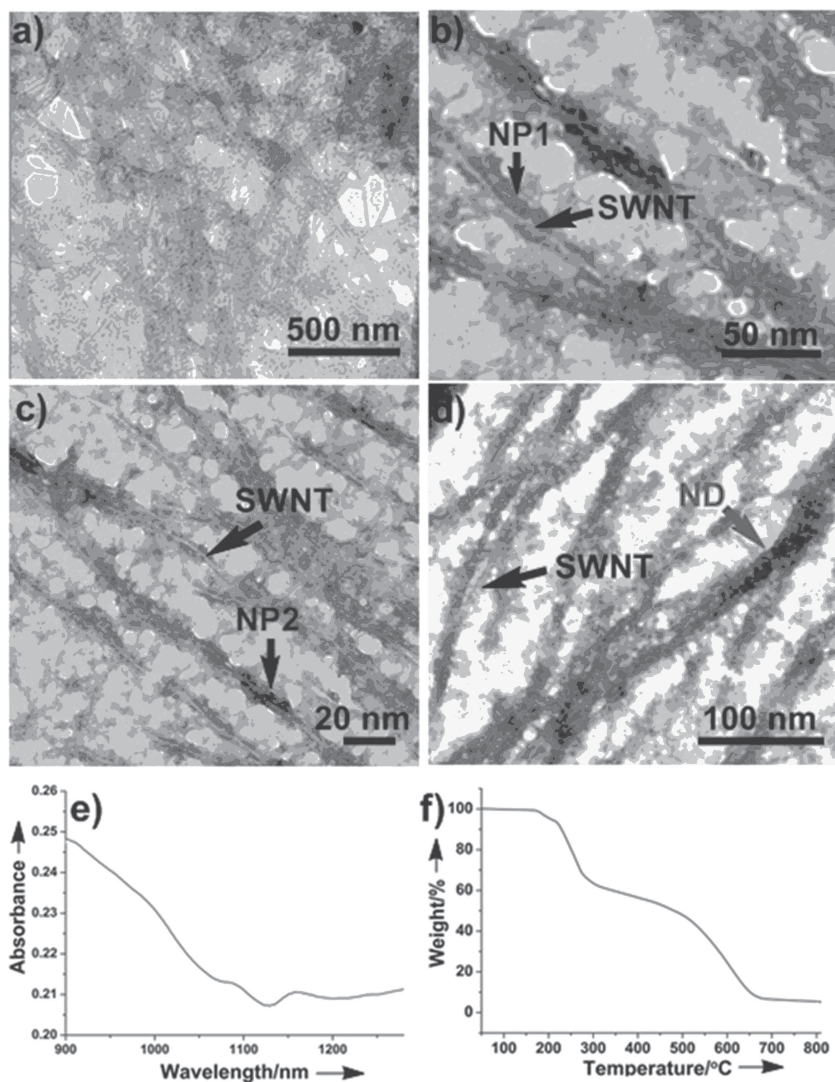


Figure 3. TEM images of a) SWNTs, b) NP1/SWNTs, c) NP2/SWNTs, and d) ND/SWNTs. e) UV-Vis-NIR spectrum of the NP1/SWNTs hybrid. f) TGA curve of the NP1/SWNTs hybrid.

utilized to confirm whether *E. coli* agglutination was induced by NP1, NP2, and ND. Only a few *E. coli* cells were in contact with each other, indicating an extremely low agglutination ability of the bolaform amphiphiles alone in the monovalent binding mode (Figure 4c, f, i), presumably because the length of the aggregates formed by the bola-amphiphiles themselves was too short to agglutinate *E. coli* cells.^[11c] Contrarily, the sizes of bacterial clusters that incubated with the hybrid materials observed in fluorescence images were quite large (Figure 5a, e, i and Figure 5b, f, j), indicating a high agglutination ability towards *E. coli*. TEM images with a higher resolution showed that the *E. coli* cells stacked together tightly (Figure 5c, g, k and Figure 5d, h, l), consistent with the results obtained from fluorescent images.

Spectrophotometric analysis based on turbidity or optical density (OD) is widely used to estimate the number of bacteria in liquid cultures, because the intensity of transmitted light

decreases dramatically when the population of bacterial cells increases. We determined the variation in the agglutination of *E. coli* by measuring the changes in optical density (ΔOD) at a fixed time interval (1 h). As shown in Figure 5m, normal bacterial growth curves could be observed for NP1, NP2, and ND, indicating a relatively low agglutination ability of the bolaform amphiphiles alone. The agglutination ability of ND was slightly stronger than those of NP1 and NP2, because the length of the nanorods formed by ND was longer than the diameters of the solid spherical structures formed by NP1 and NP2 (Figure 2). For the hybrid materials, the cell population in the solution containing hybrid materials decreased significantly, causing the changes in optical density (ΔOD) to be negative. This phenomenon demonstrated that the agglutination abilities of these hybrid materials were extremely high, resulting in the complete inhibition of the motility of the pathogenic cells. Furthermore, the ability of ND/SWNTs to agglutinate *E. coli* cells was better than those of NP1/SWNTs and NP2/SWNTs. The reason for this was that the galactose content in the ND/SWNTs hybrid was the highest due to stronger π - π interactions between the naphthalene diimide units and the SWNTs, as proved by the TGA analyses mentioned above. Notably, we were not able to observe any sign of disagglutination even after several days of incubation, demonstrating the high stability of the hybrid materials in the agglutinates.

Agglutination index (AI) assays were also performed to examine the ability of the hybrid materials to agglutinate the *E. coli* cells (Figure 5n). A significant difference between the hybrids and the bola-amphiphiles alone was observed in terms of the ability to agglutinate *E. coli*. The AI values reached 159, 145, and 178 for NP1/SWNTs, NP2/SWNTs, and ND/SWNTs, respectively, which is more than 20 fold the values of the corresponding bolaform amphiphiles alone (<7), showing much stronger cell agglutination. These results confirmed that the length of the aggregates played a significant role in the formation of bacterial clusters and was a crucial factor in controlling agglutination, as was also demonstrated by fluorescence microscopy, TEM, and spectrophotometric analyses.

The length of the biohybrid materials reached $\approx 30 \mu\text{m}$ due to the presence of SWNTs, which is much longer than the self-assemblies formed by the bolaform amphiphiles themselves. So the galactose-coated CNTs interconnect more *E. coli* cells than NP1, NP2, or ND, resulting in the stronger immobilization of the bacterial cells. On the other hand, apart from the π - π stacking interactions between the naphthalene (or naphthalene diimide) and the SWNTs, carbohydrates

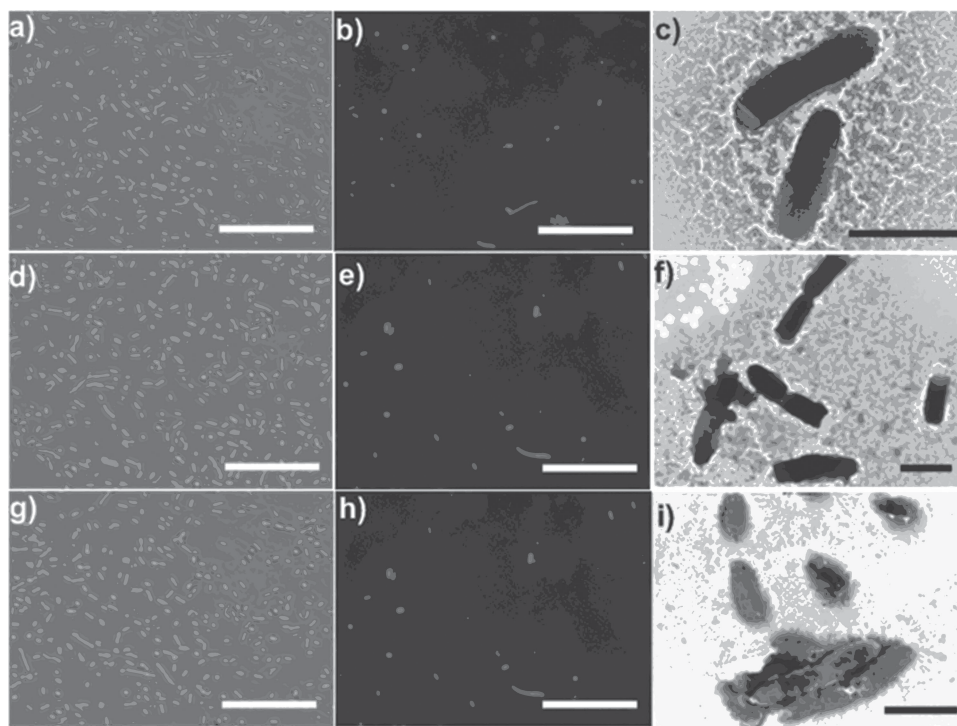


Figure 4. Microscopic images of *E. coli* agglutination incubated with **NP1**, **NP2**, and **ND**, respectively (1.50 mM): a) optical microscopic image (OMI) of **NP1**; b) fluorescence microscopic image (FMI) of **NP1**; c) TEM image (TEMI) of **NP1**; d) OMI of **NP2**; e) FMI of **NP2**; f) TEMI of **NP2**; g) OMI of **ND**; h) FMI of **ND**; i) TEMI of **ND**. For OMI images, scale bar = 40 μm . For FMI images, λ_{exc} = 360 nm, scale bar = 40 μm . For TEMI images, scale bar = 2 μm .

on both sides of the aromatic rings assist in solubilizing the SWNTs, so the stability of the hybrid materials is high enough under the experimental conditions. Their binding with the pathogenic *E. coli* for cell agglutination could be achieved effectively. Moreover, the galactoses located on the surface of the SWNTs proved to be more efficient in binding with bacterial cells, which indicated the uniqueness of the SWNTs as a semi-flexible platform for multivalent display of the monosaccharides.

In summary, three bola-amphiphiles, **NP1**, **NP2**, and **ND**, were designed and synthesized. Driven by π - π interactions and hydrophobic effects, spherical structures were obtained from the self-assembly of **NP1** or **NP2** in water, while nanorods were produced from the self-assembly of **ND**. Furthermore, three supramolecular biohybrid materials, **NP1**/SWNTs, **NP2**/SWNTs, and **ND**/SWNTs, consisting of SWNTs and the bola-amphiphiles, were successfully prepared. Compared with the aggregates formed by any of the three bola-amphiphiles, these supramolecular biohybrid materials agglutinated *E. coli* much more effectively due to the existence of rich galactose surfaces of the SWNTs, providing multivalent ligands for the carbohydrate receptors on *E. coli*. These supramolecular biohybrid materials maintained the excellent properties of the SWNTs and endowed them with interesting bioapplications at the same time. This new strategy to make CNT-based biomaterials has the potential to address many biocompatibility-

related issues, opening up an even wider range of bioapplication opportunities in areas such as drug delivery, bioconjugation, and specific recognition, including the interesting use of sugar-functionalized CNTs to bind and aggregate anthrax spores.

Experimental Section

General Methods: Solvents were either employed as purchased or dried according to procedures described in the literature. ^1H and ^{13}C NMR spectra were collected on a Bruker Avance DMX-500 spectrometer with TMS as an internal standard. UV-vis spectra were obtained using a Shimadzu UV-2550 UV-vis spectrophotometer. The fluorescence experiments were conducted on a RF-5301 spectrofluorophotometer (Shimadzu Corporation, Japan). TEM investigations were carried out on a HT-7700 instrument. The CAC values of the bolaform amphiphiles were determined on a DDS-307 instrument (Shanghai Precision & Scientific Instrument Co., Ltd.). UV-vis-NIR spectra were obtained using a Shimadzu UV-3150 spectrophotometer. Mass spectra were obtained on a Bruker Esquire 3000 plus mass spectrometer (Bruker-Franzen Analytik GmbH Bremen, Germany) equipped with an electrospray ionization (ESI) interface and an ion trap analyzer. High resolution mass spectrometry was performed on a WATERS GCT Premier mass spectrometer. DLS measurements were carried out using a 200 mW polarized laser source Nd:YAG ($\lambda = 532$ nm). The polarized scattered light was collected at 90° in a self-beating mode with a Hamamatsu R942/02 photomultiplier. The signals were sent to a Malvern 4700 submicrometer particle analyzer system.

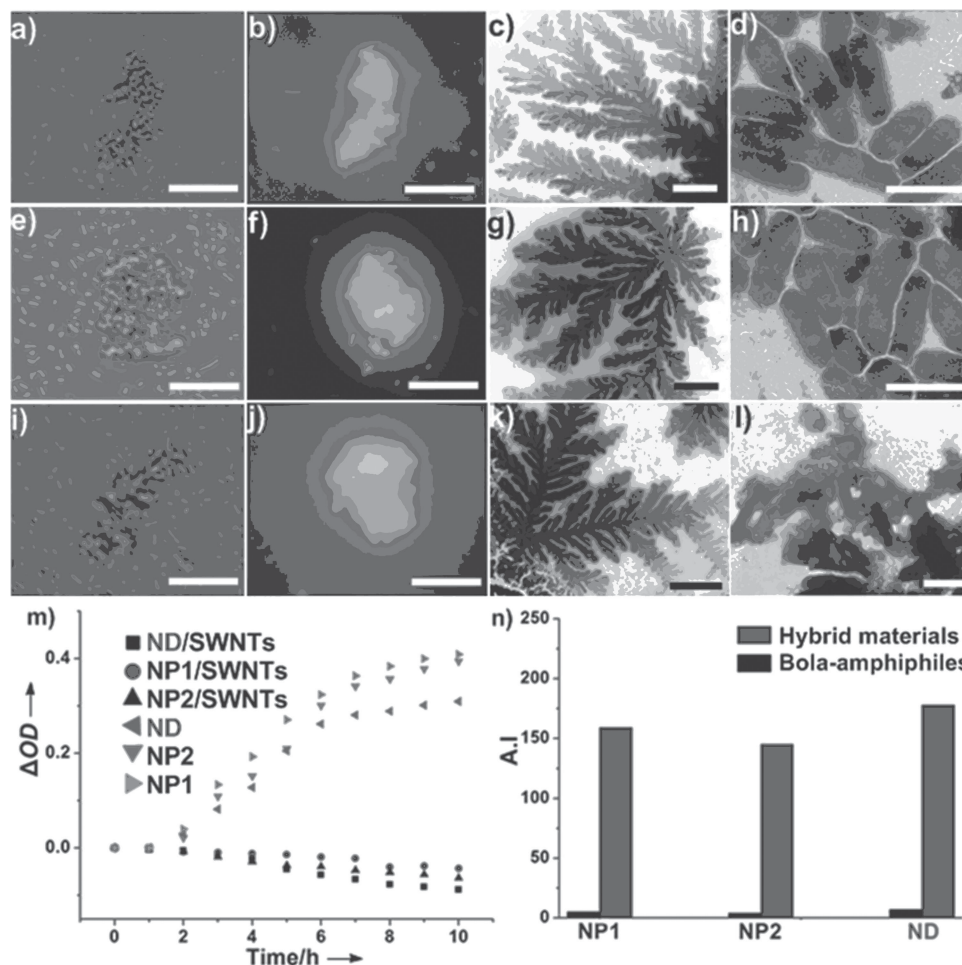


Figure 5. Microscopic images of *E. coli* agglutination incubated with NP1/SWNTs, NP2/SWNTs, and ND/SWNTs: a) optical microscopic image (OMI) of NP1/SWNTs; b) fluorescence microscopic image (FMI) of NP1/SWNTs; c) TEM image (TEMI) of NP1/SWNTs; d) enlarged image of c; e) OMI of NP2/SWNTs; f) FMI of NP2/SWNTs; g) TEMI of NP2/SWNTs; h) enlarged image of g; i) OMI of ND/SWNTs; j) FMI of ND/SWNTs; k) TEMI of ND/SWNTs; l) enlarged image of k. For OMI images, scale bar = 40 μm . For FMI images, $\lambda_x = 360 \text{ nm}$, scale bar = 40 μm ; For TEMI images, scale bar = 5 μm ; enlarged TEM images, scale bar = 2 μm . m) Growth curves based on the optical density at 600 nm for *E. coli* grown in the presence of NP1, NP2, and ND, and their corresponding hybrid materials. n) Agglutination index obtained from fluorescence microscopy and TEM images.

Supporting Information

Supporting Information is available from the Wiley Online Library or from the author.

Acknowledgements

This work was supported by National Basic Research Program (2013CB834502), the National Natural Science Foundation of China (91027006 and 21125417), and the Fundamental Research Funds for the Central Universities (2012QNA3013).

Received: June 28, 2013

Revised: July 26, 2013

Published online: September 1, 2013

[1] a) A. M. Fennimore, T. D. Yuzvinsky, W.-Q. Han, M. S. Fuhrer, J. Cumings, A. Zettl, *Nature* **2003**, 424, 408; b) N. W. S. Kam, M. O'Connell, J. A. Wisdom, H. Dai, *Proc. Natl. Acad. Sci. USA*

- 2005**, 102, 11600; c) G. A. Rivas, M. D. Rubianes, M. C. Rodríguez, N. F. Ferreyra, G. L. Luque, M. L. Pedano, S. A. Miscoria, C. Parrado, *Talanta* **2007**, 74, 291; d) Y.-L. Zhao, L. Hu, J. F. Stoddart, G. Grüner, *Adv. Mater.* **2008**, 20, 1910; e) C. Backes, F. Hauke, A. Hirsch, *Adv. Mater.* **2008**, 20, 939; f) F. Lu, L. Gu, M. J. Meziani, X. Wang, P. G. Luo, L. M. Veca, L. Cao, Y.-P. Sun, *Adv. Mater.* **2009**, 21, 139.
- [2] a) L. Gu, T. Elkin, X. Jiang, H. Li, Y. Lin, L. Qu, T.-R. J. Tzeng, R. Joseph, Y.-P. Sun, *Chem. Commun.* **2005**, 874; b) D. M. Guldi, G. M. A. Rahman, F. Zerbetto, M. Prato, *Acc. Chem. Res.* **2005**, 38, 871; c) X. Peng, S. S. Wong, *Adv. Mater.* **2009**, 21, 625; d) X. Zhou, F. Boey, H. Zhang, *Chem. Soc. Rev.* **2011**, 40, 5221.
- [3] a) J.-M. Nam, M. A. Ratner, X. Liu, C. A. Mirkin, *J. Phys. Chem. B* **2003**, 107, 4705; b) X. Chen, G. S. Lee, A. Zettl, C. R. Bertozzi, *Angew. Chem. Int. Ed.* **2004**, 43, 6111; c) H. G. Sudibya, J. Ma, X. Dong, S. Ng, L.-J. Li, X.-W. Liu, P. Chen, *Angew. Chem. Int. Ed.* **2009**, 48, 2723; d) Y. Ding, S. Chen, H. Xu, Z. Wang, X. Zhang, *Langmuir* **2010**, 26, 16667; e) G. Yu, M. Xue, Z. Zhang, J. Li, C. Han, F. Huang, *J. Am. Chem. Soc.* **2012**, 134, 13248.
- [4] a) H. Hu, Y. C. Ni, S. K. Mandal, V. Montana, N. Zhao, R. C. Haddon, V. Parpura, *J. Phys. Chem. B* **2005**, 109, 4285; b) X. Han, Y. Li,

- Z. Deng, *Adv. Mater.* **2011**, *23*, 4805; c) E. Dillon, M. S. Bhutani, A. R. Barron, *J. Mater. Chem. B* **2013**, *1*, 1461.
- [5] G. Yu, X. Zhou, Z. Zhang, C. Han, Z. Mao, C. Gao, F. Huang, *J. Am. Chem. Soc.* **2012**, *134*, 19489.
- [6] a) K. Liu, C. Wang, Z. Li, X. Zhang, *Angew. Chem. Int. Ed.* **2011**, *50*, 4952; b) K. Liu, Y. Yao, C. Wang, Y. Liu, Z. Li, X. Zhang, *Chem. Eur. J.* **2012**, *18*, 8622.
- [7] a) H. W. Gibson, H. Marand, *Adv. Mater.* **1993**, *5*, 11; b) C. A. Schalley, *Adv. Mater.* **1999**, *11*, 1535; c) J. A. A. W. Elemans, R. van Hameren, R. J. M. Nolte, A. E. Rowan, *Adv. Mater.* **2006**, *18*, 1251; d) C. Schmuck, W. Wienand, *Angew. Chem. Int. Ed.* **2001**, *40*, 4363; e) F. Wang, J. Zhang, X. Ding, S. Dong, M. Liu, B. Zheng, S. Li, L. Wu, Y. Yu, H. W. Gibson, F. Huang, *Angew. Chem. Int. Ed.* **2010**, *49*, 1090; f) Z. Zhang, Y. Luo, J. Chen, S. Dong, Y. Yu, Z. Ma, F. Huang, *Angew. Chem. Int. Ed.* **2011**, *50*, 1397; g) G. Gröger, W. Meyer-Zaika, C. Böttcher, F. Gröhn, C. Ruthard, C. Schmuck, *J. Am. Chem. Soc.* **2011**, *133*, 8961; h) X. Yan, D. Xu, X. Chi, J. Chen, S. Dong, X. Ding, Y. Yu, F. Huang, *Adv. Mater.* **2012**, *24*, 362.
- [8] a) K. E. Jones, N. Patel, M. Levy, A. Storeygard, D. Balk, J. Gittleman, P. Daszak, *Nature* **2008**, *451*, 990; b) D. I. Andersson, D. Hughes, *Nat. Rev. Microbiol.* **2010**, *8*, 260; c) C. Zhu, Q. Yang, L. Liu, F. Lv, S. Li, G. Yang, S. Wang, *Adv. Mater.* **2011**, *23*, 4805; d) M.-H. Xiong, Y.-J. Li, Y. Bao, X.-Z. Yang, B. Hu, J. Wang, *Adv. Mater.* **2012**, *24*, 6175; e) T. R. Branson, W. B. Turnbull, *Chem. Soc. Rev.* **2013**, *42*, 4613.
- [9] a) P. M. Rudd, T. Elliott, P. Cresswell, I. A. Wilson, R. A. Dwek, *Science* **2001**, *291*, 2370; b) M. D. Disney, J. Zheng, T. M. Swager, P. H. Seeberger, *J. Am. Chem. Soc.* **2004**, *126*, 13343; c) P. R. Crocker, J. C. Paulson, A. Varki, *Nat. Rev. Immunol.* **2007**, *7*, 255; d) S. Park, M.-R. Lee, I. Shin, *Chem. Soc. Rev.* **2008**, *37*, 1579.
- [10] a) H. Rüdiger, H.-J. Gabius, *Glycoconjugate J.* **2001**, *18*, 589; b) M. M. Fuster, J. D. Esko, *Nat. Rev. Cancer* **2005**, *5*, 526; c) Y. van Kooyk, G. A. Rabinovich, *Nat. Immunol.* **2008**, *9*, 593.
- [11] a) M. D. Disney, J. Zheng, T. M. Swager, P. H. Seeberger, *J. Am. Chem. Soc.* **2004**, *126*, 13343; b) J.-H. Ryu, E. Lee, Y. Lim, M. Lee, *J. Am. Chem. Soc.* **2007**, *129*, 4808; c) D.-W. Lee, T. Kim, I.-S. Park, Z. Huang, M. Lee, *J. Am. Chem. Soc.* **2012**, *134*, 14722.